Marine Pollution Bulletin 150 (2020) 110805

Contents lists available at ScienceDirect

Marine Pollution Bulletin

journal homepage: www.elsevier.com/locate/marpolbul

On the transport and landfall of marine oil spills, laboratory and field observations

Guillaume Novelli[a,*], Cédric M. Guigand[a], Michel C. Boufadel[b], Tamay M. Özgökmen[a]

[a] University of Miami, Rosenstiel School of Marine and Atmospheric Science, 4600 Rickenbacker Causeway, Miami, FL, USA
[b] Center for Natural Resources Development and Protection, Department of Civil and Environmental Engineering, The New Jersey Institute of Technology, Newark, NJ, USA

ARTICLE INFO

Keywords:
Oil spill
Drifters
Transport
Gulf of Mexico
Landfall
Waves

ABSTRACT

The dynamics of crude oil and different surface ocean drifters were compared to study the physical processes that govern the transport and landfall of marine oil spills. In a wave-tank experiment, drifters with drogue did not follow oil slicks. However, patches of undrogued drifters and thin bamboo plates did spread at the same rate and in the same direction as the crude oil slicks. Then, the trajectories of the Deepwater Horizon oil spill and 1300 drifters released near the spill source were investigated. Undrogued drifters were transported twice as fast as drogued drifters across the isobaths. 25% of the undrogued drifters landed, versus about 5% of the drogued ones, for the most part, on the same coastline locations where oil was found after Deepwater Horizon. Results highlight the importance of near surface gradients in controlling the cross-shelf transport and landing of surface material on the Gulf of Mexico's northern shores.

1. Introduction

Marine oil spills can damage the marine environment and disrupt the life and economy of coastal communities, which rely on water quality for their tourism and fishery industries. Assessing potential environmental impacts, and implementing appropriate response strategies depend on the ability to predict the path and the spread rate of an oil spill under variable weather conditions. Most spilled hydrocarbons are lighter than seawater (Wang et al., 2003), and therefore, tend to float at the sea-surface. Oil at sea mixes with water and may emulsify. Depending on the sea state and the oil composition, oil droplets may disperse over hundreds of kilometers at the surface in the form of films, slicks, or tar-balls, of thicknesses varying from tens of microns to a few centimeters (Daling et al., 2003). Therefore, the processes governing the dispersion of oil act across a range of scales of several orders of magnitude, which is too wide to be handled by the current numerical models used for prediction of trajectories in the ocean. Conducting ocean experiments by releasing oil (Faksness et al., 2016), or harmless oil surrogates such as ocean drifters (Fingas, 2011; Novelli et al., 2018), is necessary to help evaluate models (Jones et al., 2016; Reed et al., 1994), to define useful parameterizations, and to identify future directions for improvement (Reed et al., 1999; Spaulding, 2017). Few observational studies have tracked accurately oil and oil surrogates, and only on a small scale (for hours to days) (Goodman et al., 1995; Jones et al., 2016; Reed et al., 1994). These studies consistently report that drifters, with a draft of several tens of centimeters to meters—that is, much deeper than typical oil slick thickness, rapidly diverge from spilled oil even under low winds. The logistics of organizing experimental oil spills are fraught with safety and environmental concerns that ultimately limit the reasonable size and conditions under which such experiments can be conducted. As a result, a systematic and comprehensive comparison of advection and the spread of oil and drifters still needs to occur. This article intends to address this gap.

The predictability of trajectories of a tracer in the ocean is limited to a few days (Mariano et al., 2011; Piterbarg et al., 2007). In order to learn more about physical transport processes in the ocean, the Consortium for Advanced Research on the Transport of Hydrocarbons in the Environment (CARTHE) carried out a series of targeted ocean experiments where thousands of oceanic drifters were released in the Gulf of Mexico, in the area impacted by the 2010 Deepwater Horizon (DwH) oil spill. Most of the drifters released by CARTHE used a drogue to follow the horizontal current in the upper 0.50 m. However, in one of the experiments, hundreds of drifters lost their drogue (Haza et al., 2018), making this subset of drifters more directly forced by wind and waves than by sub-surface currents below 0.05 m depth. This serendipitous event provided a unique opportunity to fill the observational gap on large scale dispersion of oil compared to a diversity of drifters. The focus of this article is to understand how these different drifters move compared to oil, which is a critical step in order to use this drifter dataset to inform oil spill research.

* Corresponding author.
E-mail address: gnovelli@rsmas.miami.edu (G. Novelli).

https://doi.org/10.1016/j.marpolbul.2019.110805
Received 31 July 2019; Received in revised form 3 December 2019; Accepted 5 December 2019
Available online 10 December 2019

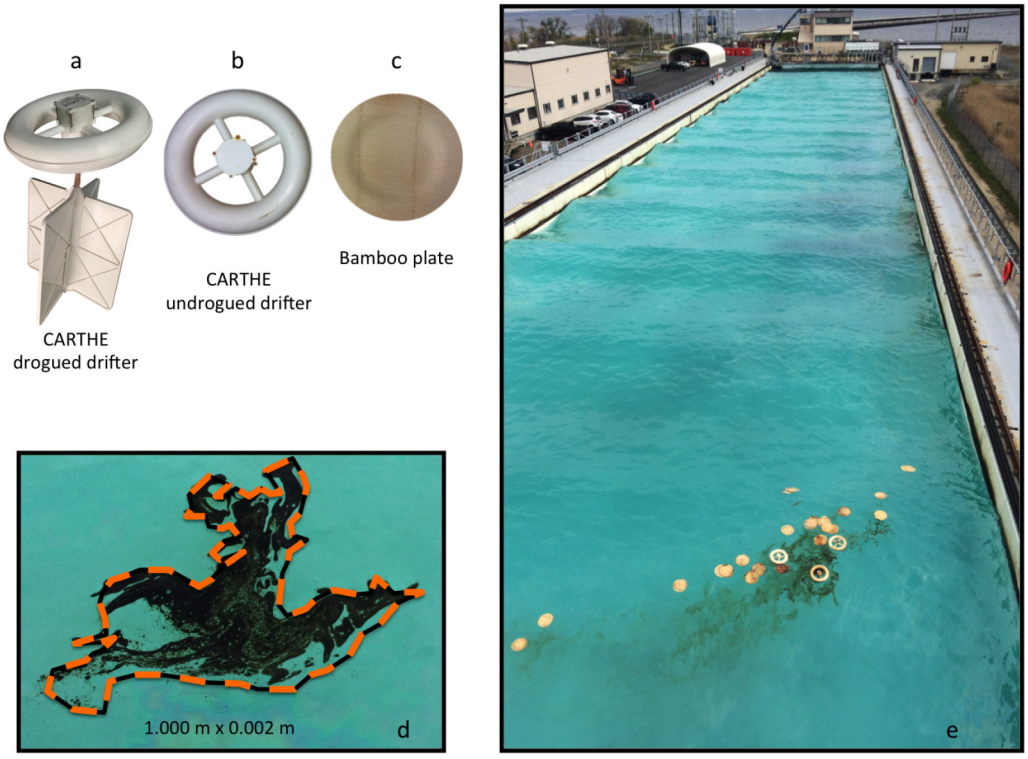

Fig. 1. (a) CARTHE drogued drifter (38 cm diameter × 60 cm draft). (b) CARTHE undrogued drifter viewed from above (5 cm draft). (c) Bamboo plate viewed from above (28 cm diameter × 1.75 cm draft). (d) An oil slick soon after release and its polygonal contour (orange dashed line). (e) Visualization of an experiment at OHMSETT. (For interpretation of the references to color in this figure legend, the reader is referred to the web version of this article.)

The CARTHE dataset contains drifter trajectories on and off the shelf, across seasons, in the northern Gulf of Mexico. 300 CODE drifters (based on Davis, 1985 drifter design) were released during the Grand Lagrangian Deployment (GLAD) around DwH in the summer of 2012 (Poje et al., 2014); 350 surf-zone drifters were deployed during the Surfzone and Coastal Oil Pathways Experiment (SCOPE) near Destin, Florida, in December 2013 (Roth et al., 2017); Over 5000 floating bamboo plates, tracked in geolocated aerial images (Carlson et al., 2018), and 1600 GPS-tracked CARTHE drifters (Novelli et al., 2017) were launched during the Lagrangian Submesoscale Experiment (LASER) located offshore near DwH in the winter of 2016, and the Submesoscale Processes and Lagrangian Analysis on the Shelf (SPLASH) campaign in the Louisiana bight during the spring of 2017. These drifters had different drafts, and were chosen to study transport processes at different depths, ranging from 1.75 cm (for the bamboo plates) down to 1 m (for the CODE drifters). The GLAD and LASER drifters were deployed in dense arrays in the vicinity of DwH to study relative dispersion. Olascoaga et al. (2013) and Beron-Vera and LaCasce (2016) highlighted the role of mesoscale flow in shaping the offshore transport of the GLAD drifters. Poje et al. (2014) and D'Asaro et al. (2018) showed that submesoscale features can dramatically enhance both dispersion and accumulation of drifters. Drifter-derived velocity statistics were found to vary strongly with bathymetry and winds (Curcic et al., 2016; Mariano et al., 2016). GLAD drifter data, combined with altimetric data, was found to improve estimates of ocean surface velocity fields (Berta et al., 2015). However, despite the fact that GLAD and LASER drifter datasets are comparable to the DwH oil spill in location, spatial extent, and duration, the full surface transport pathways between DwH and the shoreline have not yet been studied. In the study presented here, we conduct such analysis of the transport patterns of the DwH oil and drifters, focusing in particular on the transport directed towards the shore and the landing mechanisms.

During coastal field campaigns in Norway and in the Gulf of Mexico, Röhrs et al. (2012) and Laxague et al. (2018) have measured significant near-surface vertical shear in the presence of wind-waves, which resulted in the rapid separation of drogued and undrogued drifters. Reed et al. (1994) field trials indicated that oil slicks and various drifters could diverge in the presence of wind and waves. However, there is no clear measurement of the effect of waves on the motion of oil, especially in comparison to drifters, which would be valuable in order to best utilize the CARTHE drifter dataset. The drift characteristics of CODE and CARTHE drifters have been studied rather extensively (Davis, 1985; Novelli et al., 2017; Poulain and Gerin, 2019), but have never been explicitly compared to oil. Laboratory experiments have been used successfully to isolate certain processes that affect the transport of oil in the ocean, such as the effect of dispersants (Soloviev et al., 2016) and the nature of the oil discharge (Boufadel et al., 2018). Here, we present a wave-tank experiment comparing the wave-driven dispersion and advection of an oil slick with that of the same CARTHE drifters (drogued and undrogued) and bamboo plates used in the large LASER drifter dataset mentioned earlier. Oil and drifters were released side by side in a large tank, where the wave-induced component of surface transport was isolated, in order to supplement the DwH oil and CARTHE drifter trajectories collected in the Gulf of Mexico.

2. Wave-tank experiment

2.1. Material and methods

A series of experiments were conducted at the Oil Spill and Hazardous Material Simulating Test Tank facility (hereafter OHMSETT) located in Leonardo, New Jersey, to quantify how drifters move compared to oil in a controlled environment. OHMSETT is a large open-air wave tank, designed to test equipment for recovery and containment of oil and other hazardous material potentially spilled at sea. It features mechanical wave-paddles capable of generating monochromatic waves that have relatively small amplitudes (maximum 0.60 m) but cover most of the ocean wave-frequency spectrum. The dimensions of the tank, 200 m × 20 m × 2.5 m, allow the use of full-scale equipment before application in the field in challenging but controlled conditions. The tank is used mostly for industry tests and developments, but also for academic research for example involving oil releases at high Reynolds number (Zhao et al., 2016).

This experiment consisted of tracking oil and three types of drifters

released concurrently in a vertically sheared flow induced by waves and modulated by the ambient wind (see image in Fig. 1e). The oil used was a mix of Alaskan North Slope crude and Hydrocal 300, a commonly available refined oil product. Three liters of oil were released per test. The slick thickness was estimated to vary between 0.2 cm and 0.02 cm, by measuring the visible area of the slick over time. The drogued drifter, undrogued drifter, and bamboo plates from the LASER experiment, have respective drafts of 60 cm, 5.0 cm, and 1.75 cm (Fig. 1a–c).

A GoPro camera was mounted on a crane located on the instrumented bridge. The camera looked at nadir and was oriented such that the image's length was along the direction of wave propagation. The camera was controlled remotely via WiFi to launch the recording and check for the correct orientation and illumination of the frame. The field of view covered an area of 24 m × 12 m with a resolution of 1.5 × 1.5 cm^2/pixel.

Temporal variations of wind speed and direction were monitored from an anemometer located at the center of tank at 10 m height. Water surface elevation time-series were recorded via an Ultrasonic Distance Meter (UDM) located under the bridge used for deployments. The peak period T and significant wave height Hs were extracted from the surface elevation time-series.

The experiment began from an undisturbed, flat, water surface. A wave period and wave-height was selected by the controller. Once the waves were well formed (usually after the passage of the first five wave crests under the bridge), three operators rapidly placed 1 drogued drifter and 5 undrogued drifters in the middle of the tank. Then, the oil was poured in the center of the cluster of undrogued drifters. Finally, the bamboo plates were launched in and around the oil patch. Each experiment lasted 3 min before the regular wave field became contaminated by interactions with waves bouncing back from the end of the tank. However, the image analysis was stopped earlier, after the oil or bamboo plates exited the field of view of the camera, that is within 2 min.

We tested combinations of wave periods (T), between 1.4 s and 5.5 s, and significant wave heights (Hs), ranging from 9 cm to 60 cm. The analysis is based on the two cases (Table 1) where oil and drifters moved fast enough and had trajectories long enough to measure drift differences with confidence. In case 1, the wave characteristics were: Hs = 48 cm and T = 1.5 s. For deep-water waves, the theoretical surface Stokes drift velocity is $U_S = \omega k a^2$, where $\omega = 2\Pi/T$ is the angular frequency, $k = \omega^2/g$ is the wave number, and $a = H_s/2$ is the wave amplitude. For case 1 Stokes drift would be on the order of U_S = 0.4 m/s for deep-water waves. The average wind speed was 4 m/s, directed at 45° from the along-tank direction and against the direction of wave propagation. In case 2, the wave characteristics were: Hs = 72 cm and T = 2.2 s, which corresponds to a deep-water wave theoretical surface Stokes drift of U_S = 0.3 m/s. The average wind speed was 5.5 m/s, directed at 25° from the along-tank direction and against the direction of wave propagation.

The range of wave heights generated in the experiment are commonly observed in the field. Wave climatology in the Gulf of Mexico, compiled by Judt et al. (2016), reveals significant wave heights varying mostly between 0.2 m and 2.0 m, with a minimum in summer and maximum in winter (Fig. 2, panels f and h in Judt et al., 2016). The short wave periods (T < 2.5 s, or frequency > 0.4 Hz) used in the lab are representative of short fetch wind-waves. This type of high-frequency wind-waves are not measured accurately by the typical 3-m diameter discus buoys operated by the National Data Buoy Center, with a frequency cut-off point of 0.35 Hz (or T > 2.9 s) (Drennan et al., 1998). Novel optical wave observations have clearly showed that the drift speed in the upper centimeter of the ocean is strongly dependent on the Stokes drift generated by high-frequency wind-waves (Laxague et al., 2018, 2017). Studies of waves in the North Pacific (Tamura et al., 2012) and in the Gulf of Mexico (Clarke and Van Gorder, 2018) confirm that surface Stokes drift is dominated by the highest wave frequencies between approximately 0.3 Hz and 1.0 Hz; hence the relevance of the laboratory waves presented here for the study of oil slick transport.

Table 1
Summary of conditions imposed in the wave-tank experiment. The wind direction is given with respect to the direction of wave propagation.

	H_s [m]	T [s]	U_S [m/s]	U_{10} [m/s]	Wind direction [°]
Case 1	0.48	1.5	0.43	4.0	45
Case 2	0.72	2.2	0.31	5.5	25

The two cases show distinct transport patterns (Fig. 2), which may be attributed to variations in the wind direction. In the first case, the oil, undrogued drifters, and bamboo plates showed a similar advection along the direction of wave propagation, while spreading mostly across the tank in the first 90 s, after which they started elongating in the along-tank direction (Fig. 2a and b). In the second case, the oil, undrogued drifters, and bamboo plates were advected together to the right of the direction of wave propagation, but slower than in the first case. While moving against the wind, they aligned into the wind towards the top of the frame (Fig. 2c and d). In both cases, due to the absence of current below the surface, the drogued drifter did not move significantly.

Individual frames were extracted from the video files every 5 s to be able to see clearly the motion of the drifters over at least two wave periods. The frames were then rectified to eliminate the wide-angle lens barrel distortion using standard correction for GoPro camera lenses. The stack of images was imported and processed in ImajeJ (Schneider et al., 2012), a flexible open tool for scientific image analysis. The ImajeJ tracking plug-in called MtrackJ (Meijering et al., 2012) was used to retrieve individual trajectories of each drifter and selected bamboo plates. A polygon was drawn by hand around the oil slick and the equivalent ellipse properties were calculated automatically in ImageJ (position of the center of mass, length and orientation of the major and minor principal axes, σ^{oil}_{maj} and σ^{oil}_{min}). The error in position for the center of the plates or undrogued drifter is 1 pixel. The velocities were deduced by finite-differences of the positions between frames with an accuracy of 0.6 cm/s.

2.2. Results

2.2.1. Velocities

The temporal evolution of the velocities of the oil slick center of mass (CoM), as well as individual bamboo plates (5 for case 1, 10 for case 2) and undrogued drifters (5 for both cases) and their respective center of mass velocities are plotted in Fig. 3. The velocity was decomposed in the along-tank direction and the across-tank direction.

In the first case (Fig. 3a and c), the mean difference of velocity between oil and plates centers of mass was 0.4 cm/s in the along-tank direction and 0.1 cm/s in the across-tank direction, with standard deviations of 2.2 cm/s and 1 cm/s respectively. The mean difference of velocity between oil and undrogued drifters centers of mass was 0.6 cm/s in the along-tank direction and 0.2 cm/s in the across-tank direction, with standard deviations of 1.7 cm/s and 1.3 cm/s respectively. Based on a mean oil velocity in the along-tank direction of 8.8 cm/s, these results are equivalent to differences of velocities between the oil and the plates of 4.5%, and 6.8% between the oil and the undrogued drifters.

In the second case (Fig. 3b and d), the mean difference of velocity between oil and plates centers of mass was 2 cm/s in the along-tank direction and 1.5 cm/s in the across-tank direction, with standard deviations of 4.9 cm/s and 3.3 cm/s respectively. The mean difference of velocity between oil and undrogued drifters centers of mass was 0.1 cm/s in the along-tank direction and 0.1 cm/s in the across-tank direction, with standard deviations of 4.8 cm/s and 3.5 cm/s respectively. In case 2, despite a visually good match between plates, undrogued drifters and oil slick motion, a larger velocity difference was

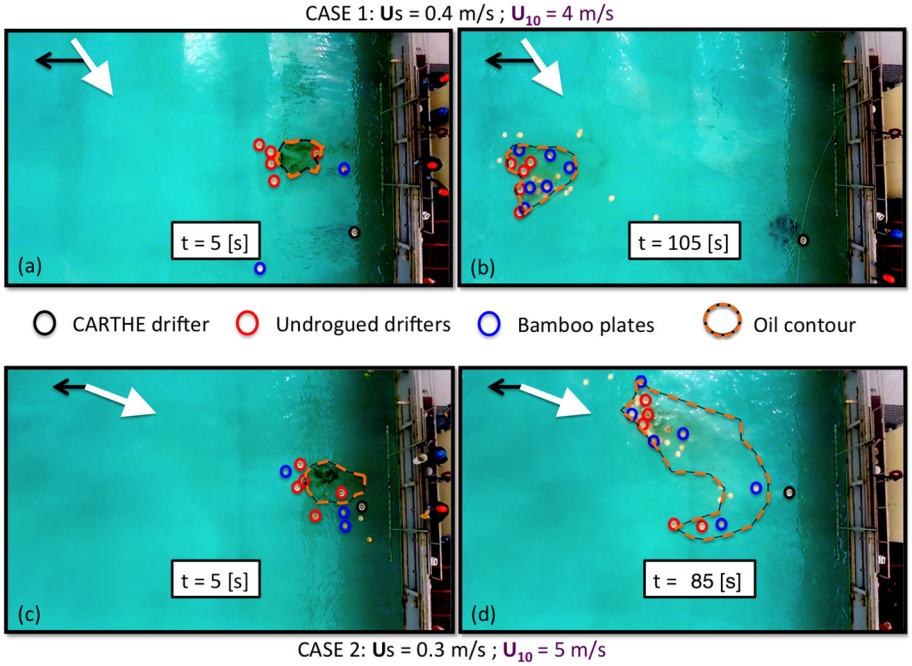

Fig. 2. Snapshots at the beginning (a, c) and end (b, c) of case 1 and case 2 experiments. Black arrows represent the surface Stokes drift vector. White arrows represent the wind vector.

measured. The reason is that the oil center of mass position is calculated from the contour of the oil and assuming the oil had the same thickness in the whole patch. However, this assumption did not hold as well in the second experiment as it did in the first experiment. As can be seen in Fig. 2d, the thickest part of the oil moved towards the top of the frame, just like most of the plates did.

2.2.2. Absolute dispersion

From individual particle trajectories (particles referring to undrogued drifters or bamboo plates in this case), the absolute dispersion $A^2(t)$ can be measured as the mean square displacements of particles relative to their starting position ($r(t = 0)$) as per:

$$A^2(t) = < (r(t) - r(t = 0))^2 > \quad (1)$$

where the brackets $< >$ represent the mean over all the particles, and $r(t)$ is the trajectory of a particle. The absolute dispersion varies with both the drift of particles from their starting location and the spread of the particles about their center of mass. The absolute dispersion of the undrogued drifters and bamboo plates for both cases 1 and 2 is plotted as a function of time in Fig. 4. The square displacement of the center of mass of the oil slick is also plotted for reference. At early times, the absolute dispersion is expected to grow quadratically in time (LaCasce, 2008). It reflects that transport is dominated by advection (over diffusion) at this time scale. In each case,the absolute dispersion of undrogued drifters, bamboo plates, and oil have similar trend. However, the absolute dispersion in case 1 is about one order of magnitude higher than in case 2, most likely because in the first case a stronger Stokes drift, motor of the advection, led to larger displacements. The absolute dispersion varies quadratically in time for case 1. The absolute dispersion of the bamboo plates in case 2 grows faster in time than the rest, which might be related to the initial release of the plates.

In summary, on one hand, the drogued drifter remained stationary, insensitive to the wave- and wind-induced surface current. On the other hand, the oil, undrogued drifters, and bamboo plates, moved in the same direction and at the same speed. The maximum difference of velocity between the oil slicks and the undrogued drifters and plates was estimated to be 2 cm/s. The drastic difference between the advection of drogued drifters and oil/undrogued drifters/bamboo plates

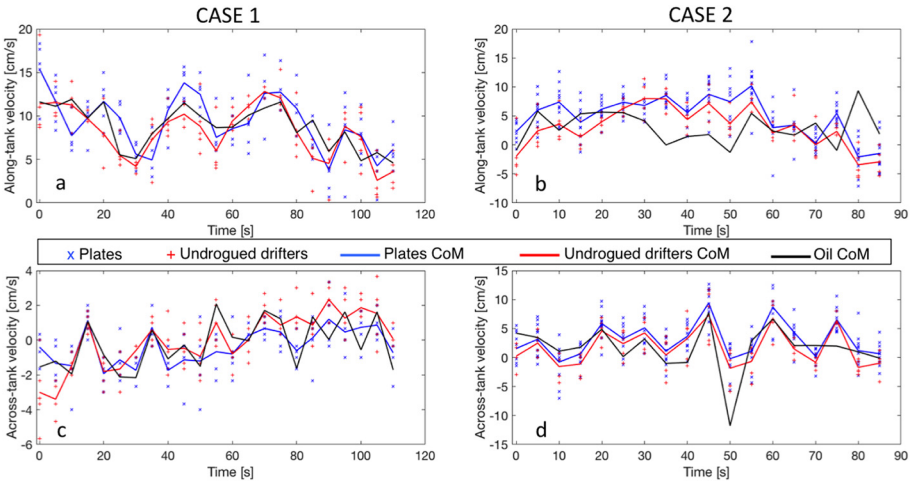

Fig. 3. Along-tank (a, b) and across-tank (c, d) velocity time-series for case 1 and case 2 experiments. Solid lines are the velocities of the center of mass of oil in black, bamboo plates in blue, and undrogued drifters in red. (For interpretation of the references to color in this figure legend, the reader is referred to the web version of this article.)

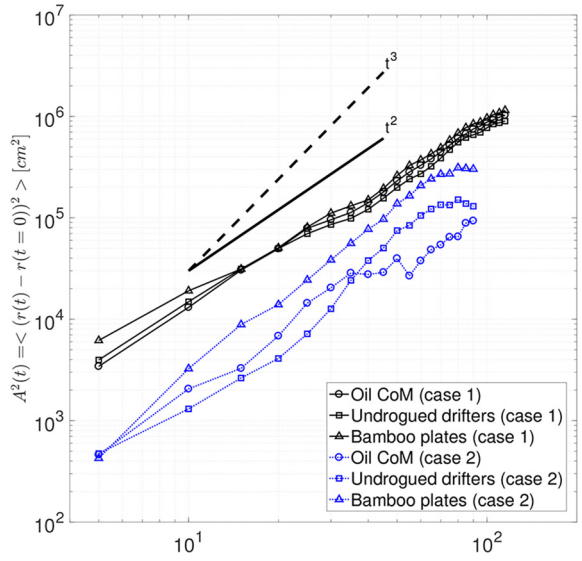

Fig. 4. Absolute dispersion measured for case 1 (black solid lines) and case 2 (blue dash-dot lines). □ undrogued drifters, △ bamboo plates, and ∘ oil slick center of mass. $A^2(t) \sim t^2$ and $A^2(t) \sim t^3$ are indicated in solid and dashed black lines. (For interpretation of the references to color in this figure legend, the reader is referred to the web version of this article.)

can be attributed to the rapidly depth-decaying near-surface shear induced by Stokes drift and wind stress. A larger number of particles and estimates of the oil slick thickness would be necessary to reduce the uncertainty in the velocity measurements.

2.2.3. Pair separation

The statistical properties of the distribution of a cloud of tracer quantify the relative motion of a tracer about its center of mass. Fig. 5 shows, for case 1 and 2, the evolution of the distribution of pair separations (in 25 cm bins every 5 s) of undrogued drifters (Fig. 5a and c), and bamboo plates (Fig. 5b and d). The shades of gray represent the number of pairs in each bin, larger number of pairs being darker. The initial distributions have pair separations varying between 0 and 5 m. Over time some gray bands move downward indicating clustering, while other gray bands move upward, reflecting pairs separating from each other. In other words, some areas accumulate tracers, and an empty space is left in between the accumulation regions. Fig. 5c is the clearest example of this evolution. The RMS separation is overlaid in solid lines. RMS separation growth over time is a traditional metric to describe relative dispersion (LaCasce, 2008). However, the RMS separation growth shows little to no dispersion in both cases. The length of the principal axis of elongation of the oil slick ellipse is $2\sigma^{oil}_{maj}$. Its temporal evolution matches closely the maximal separation of pairs (uppermost gray bands) of both undrogued drifters and bamboo plates, but only when the initial maximal separation of particle pairs matched the initial size of the oil ellipse.

2.2.4. Principal direction of relative dispersion and anisotropy

The orientation of the principal major axis of dispersion of the tracer distributions is measured by Θ with respect to the direction of wave propagation (see insert in Fig. 6c). The evolution of Θ is presented in Fig. 6a and b for cases 1 and 2. Unfortunately, this measure is very sensitive to the number of bamboo plates (or undrogued drifters) in the ensemble. At short time scales, it is also quite sensitive to the initial distribution of the ensemble: the relative positions of the particles at the end of the experiment is still correlated to their initial relative positions. Therefore, it is only meaningful to compare Θ for the oil and bamboo plates for case 2, because 45 pairs of bamboo plates were used (versus 5 pairs in case 1, and 5 pairs of undrogued drifters in both cases). Fig. 6b shows that, about 40 s after deployment, the oil and bamboo plate patches both elongated in the same direction (RMS difference is 3°).

The aspect ratio AR, where $AR = \frac{\sigma_{maj}}{\sigma_{min}}$, is a measure of the anisotropy of the diffusion process. The lower panels of Fig. 6c and d, show the evolution of AR for cases 1 and 2. Like Θ, to be accurate, this metric

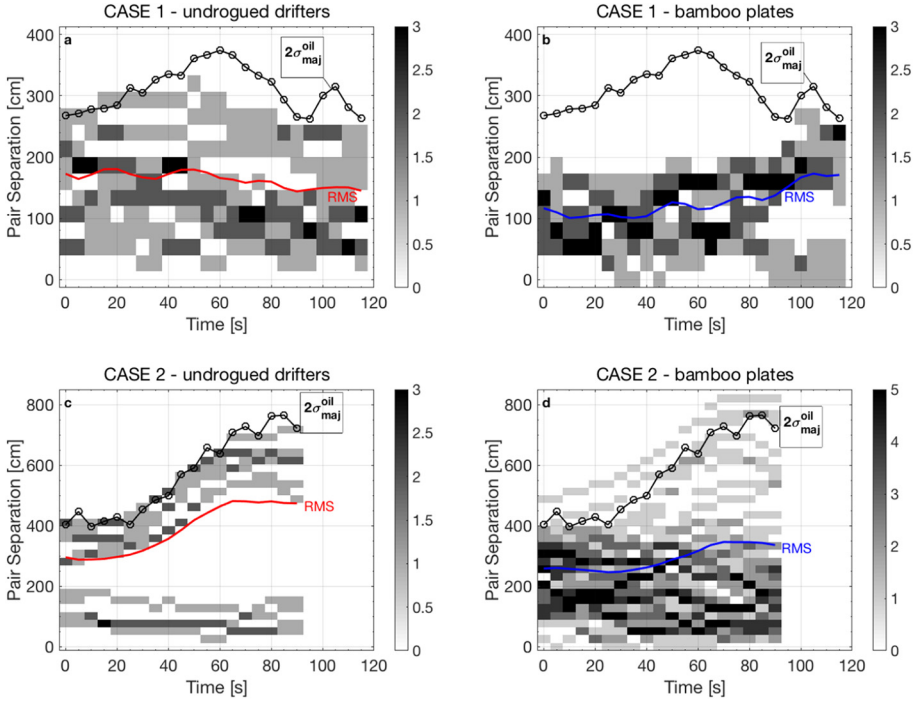

Fig. 5. Distribution of undrogued drifters and bamboo plates pair separations as a function of time (gray shading indicates the number of pairs in each bin) for case 1 (a, b) and case 2 (c, d). RMS pair separation is shown in solid red (resp. blue) line for the undrogued drifters (resp. bamboo plates). The length $2\sigma^{oil}_{maj}$ of the principal axis of elongation of the oil slick ellipse is indicated in black lines with ∘. (For interpretation of the references to color in this figure legend, the reader is referred to the web version of this article.)

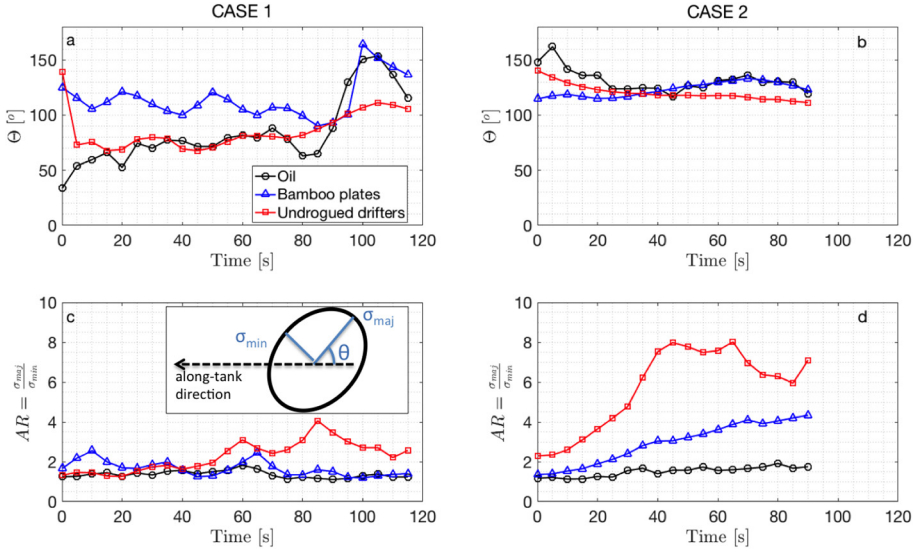

Fig. 6. Direction of the major axis of dispersion (Θ) and aspect ratio ($AR = \frac{\sigma_{maj}}{\sigma_{min}}$) as a function of time for case 1 (a, c) and case 2 (b, d). Undrogued drifters in red □, bamboo plates in blue △, and oil slick in black ∘. The definitions of Θ, σ_{maj}, and σ_{min}, are indicated in the sketch inserted in panel (c). (For interpretation of the references to color in this figure legend, the reader is referred to the web version of this article.)

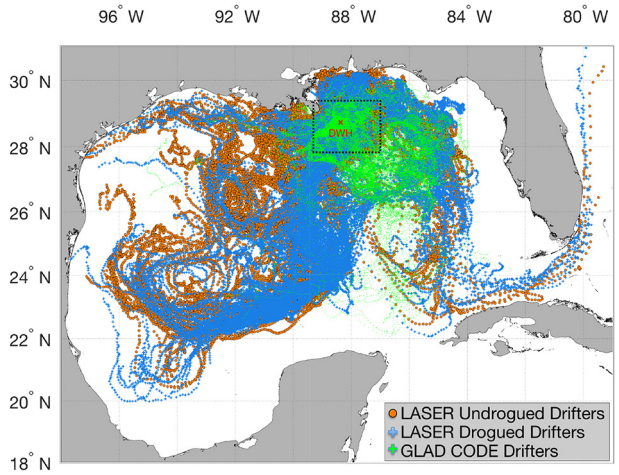

Fig. 7. Drifter positions (subsampled every 6 h) from the GLAD experiment in green (July to October 2012), and the LASER experiment (January to May 2016). LASER undrogued drifters are in orange, LASER drogued drifters are in blue. The red X marks the location of the Deepwater Horizon (DWH) wellhead in 2010. The dotted black box shows the area where the drifters were released. (For interpretation of the references to color in this figure legend, the reader is referred to the web version of this article.)

ideally requires a large number of particles evenly distributed at initial time. We thus limit our comments to the oil slick and the bamboo plate AR in case 2. In case 2, the bamboo plate's AR increased steadily over time from 1.3 to 4.3. The patch of plates was elongating much faster in the direction indicated by Θ (~120°) than across it, stretching into a line. The oil's AR had a different behavior. In case 2 it was growing slowly from 1.2 to 1.8. The growth of the oil patch was then more isotropic than the growth of the bamboo plate patch. This suggests that different processes are acting on the diffusion of the oil and the bamboo plates. One possible explanation could be that, in addition to diffusion caused by the turbulence of the surface boundary layer flow, the fresh oil lens is spreading in a so-called gravity-viscosity-surface tension regime. Fay (1971) and Hoult (1972) first described the isotropic increase of area over time of a fresh, non-weathered, thick oil slick on a water surface at rest, where oil forms a layer of uniform thickness under the balance of gravity, viscosity and ultimately surface tension. Reed et al. (1999) and Daling et al. (2003) reported that, during marine oil spills, the gravity-viscosity-surface tension spreading regime only affects fresh oil in the first hours of the oil being spilt, after which oil weathering (mostly via evaporation and emulsification) causes this spreading regime to stop. Also, this centimeter-scale diffusion process does not dominate the dispersion of slicks with characteristic length larger than hundreds of meters. Such spreading mode is obviously absent for the drifters and plates, but could have contributed significantly to extending the fresh oil slick area in all directions in our laboratory scale experiment. Thus, plates and undrogued drifters could be appropriate oil surrogates for transport studies of large weathered oil slicks in the ocean.

This laboratory-scale experiment isolated the case of surface transport induced by steep waves in the absence of underlying currents. In these limited conditions, we found that undrogued drifters and bamboo plates follow oil slicks more closely than drogued drifters. However, in the upper ocean, surface transport is subject to a full spectrum of multi-scale interactions between waves, wind, and currents, that cannot be replicated in the tank. Surface drift must be investigated in the field as well, and over periods longer than a few minutes. In the next section we will compare the fate of surface oil from the Deepwater Horizon accident to hundreds of trajectories of drogued and undrogued drifters, that were released in the vicinity of the source of the oil spill in the Northern Gulf of Mexico.

3. Ocean observations of oil and drifters transport pathways: from Deepwater Horizon to shore

3.1. GLAD and LASER drifter datasets

Fig. 7 shows the cumulative trajectories of the drifters released during the Grand Lagrangian Deployment (GLAD) and the Lagrangian Submesoscale Experiment (LASER) oceanographic campaigns carried out by CARTHE. All drifters were released within the rectangle contoured in dash black, that is in the vicinity of the DwH oil rig, to study the circulation and dispersion of floating pollutant in this area. The GLAD dataset used here contains 297 CODE drifter trajectories (in green in Fig. 7). The CODE is a standard oceanic drifter that has a drogue that spans vertically the upper 1 m, designed by Davis in the early 1980s (Davis, 1985), to represent the average current near the surface (~0.5 m deep) with very small wind-induced slip error (0.1% of

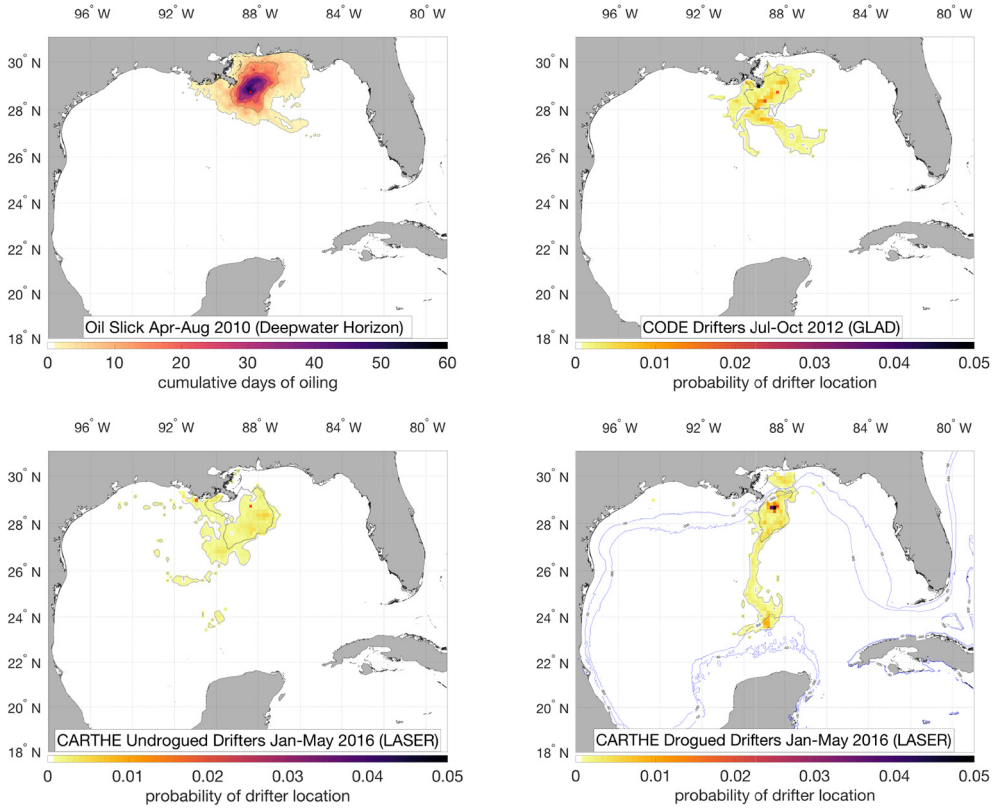

Fig. 8. Top left: Map of cumulative days of oiling (black contours every 10 days) detected by TCNNA SAR during the Deepwater Horizon oil spill in the summer of 2010 (Garcia-Pineda et al., 2013). Maps of probability density of drifters after being released at Deepwater Horizon location (red cross): dotted contours 7 days after release, and gray contour and color-coded bins 30 days after release. Top right: GLAD drifters, summer of 2012. Bottom left: LASER undrogued drifters; Bottom right: LASER drogued drifters, winter of 2016. Blue contour lines show the location of the shelf slope between the 50 m and the 300 m isobaths. (For interpretation of the references to color in this figure legend, the reader is referred to the web version of this article.)

the wind speed). The drifter trajectories, with an initial temporal resolution of 5 min and nominal spatial accuracy of 6.4 m, were low-pass filtered and spline-interpolated at regular 15 min interval (Yaremchuk and Coelho, 2015).

The LASER dataset used here has 1002 CARTHE drifter trajectories. But there are two types of drifters: 535 drogued drifters (in blue in Fig. 7) and 467 undrogued drifters (in orange in Fig. 7). Out of initially 956 drogued drifters, 421 lost their drogue during the passage of severe winter storms, and 46 additional drifters were released directly undrogued as a control group to test the drogue-detection algorithm (Haza et al., 2018). The density of data, and the altered signal transmission of the undrogued drifters, allowed for accurate detection of the moment when the drifters lost their drogue (Haza et al., 2018). The CARTHE drifters were designed to track near-surface currents near 0.5 m depth like the CODE drifters, but also to be biodegradable and inexpensive, for massive deployments (Novelli et al., 2017). Their drift was thoroughly calibrated, and proved to be virtually identical to that of CODE drifters, which makes CODE and CARTHE drifters interchangeable in experiments. The undrogued CARTHE drifters were subject to the same tests: They follow well the current in the upper 5 cm for low wind speeds (less than 5 m/s in Laxague et al., 2018), with a wind-induced slip error lower than 2% of the wind speed for wind speeds between 8 and 15 m/s (Novelli et al., 2017).

The GLAD experiment was carried out in the summer of 2012, while the LASER experiment occurred in the winter of 2016. Atmospheric forcing in this area is strongly seasonal (Judt et al., 2016): In summer, the time-averaged winds are weak (less than 5 m/s), dominated by an anticyclonic circulation such that the northern coast from Louisiana to Florida is under south- to southwesterly winds (blowing towards the shore). A notable exception to this pattern is the infrequent, irregular, and short, passage of hurricanes and tropical storms (2 hurricanes per year in average). Hurricane Alex crossed the southwestern part of the Gulf between Campeche, Mexico, and the south of the Texas border, causing disruptions during the cleanup of the oil spill in June 2010. Hurricane Isaac crossed the Gulf in straight line from Key West, Florida, to its final landing South-East of New-Orleans Louisiana, after passing over most of the GLAD drifters, in August 2012 (Curcic et al., 2016). During the winter, the mean wind pattern reverses, with strong easterly to north-easterly winds (blowing away from the shore). Wintertime weather also shows more variability with, in average, the passage of 8–9 cold fronts (or winter storms) in December, associated with the highest wind speeds and significant wave heights of the year in average, except during hurricanes (Judt et al., 2016).

As can be seen in Fig. 7, the originality of these datasets is the great density of both surface (undrogued drifters ~0.05 m deep) and near-surface measurements (drogued drifters ~0.5 m deep) at the same time and location during LASER, and at different seasons comparing GLAD and DwH in summer with LASER drogued and undrogued in winter.

3.2. Deepwater Horizon oil data

The Environmental Response Management Application (ERMA) Gulf of Mexico is a web-based Geographic Information System (GIS) that compiles many layers of data to support environmental and severe-weather responses in the Gulf of Mexico (https://erma.noaa.gov/gulfofmexico/erma.html). The National Ocean and Atmosphere Administration (NOAA) collected various products, during the Deepwater Horizon event (DwH), in relation to the extent of the oil spill over time and to where oil was found stranded on the beach. We use the "cumulative daily Synthetic Aperture Radar analysis" that assembles all the daily polygons of oil slicks detected in Synthetic Aperture Radar (SAR) imagery with a Texture Classifying Neural Network Algorithm (TCNNA). The TCNNA was developed initially by Garcia-Pineda et al. (2009) to study natural oil seeps. In 2010, the algorithm was adapted to deal with the specific signal of the massive oil spill (Garcia-Pineda et al., 2013). With 1 to 13 SAR passes per day, the patches of surface oil were quickly and reliably delineated by day or night, without being affected by cloud cover, which gives more temporal coverage compared with optical satellite images such as the ones obtained from the Moderate Resolution Imaging Sprectroradiometer (MODIS): in this SAR dataset

oil was observed 89 days, compared to 58 days with valid cloud-free MODIS images (Hu et al., 2011). The TCNNA was found to be accurate when wind speed was higher than 3 m/s, and the incidence angle were in the range from 15 to 45°. Greater details about this method can be found in Garcia-Pineda et al. (2009) and (Garcia-Pineda et al., 2013). For our purpose, the raw 50-m resolution dataset was converted to a raster map of the GoM with a spatial resolution of 5km, where each bin contains the cumulative days of oil detected in each bin over 89 days between 23 April 2010 and 11 August 2010. This data is presented in the top left panel of Fig. 8.

The oiling of the shoreline was monitored by the Shoreline Cleanup Assessment Technique (SCAT) program. 18 SCAT teams surveyed over 7000 km of shorelines, delineating and categorizing the oiling characteristics across beaches and marches of the states of Louisiana, Mississippi, Alabama, and Florida. Quality controlled data is publicly available via the ERMA GoM website, in the form of shapefiles that contain the locations surveyed along the shore, their shape (segments and polygons), and the degree of oiling (no oil observed, trace, very light, light, moderate, heavy). Details on the extent and degree of shoreline oiling related to DwH oil spill can be found in Michel et al. (2013) and Nixon et al. (2016). In this study, we considered only 2° of oiling: oil or no oil observed. Fig. 9 shows in black the areas where oil was found.

3.3. Comparative transport starting from Deepwater Horizon

Not all drifters were released from the same location at the same time. In order to compare transport pathways starting from the Deepwater Horizon platform, we compute a probabilistic transit model based on each drifter dataset that allows to propagate the drifter density from the specific location of the DwH platform. This technique has been used previously, for example to determine the location of the great garbage patches from the global set of trajectories of over 10,000 drifters released by the Global Drifter Program (GDP) (Maximenko et al., 2012). More recently, this approach was used by Miron et al. (2017) to describe the Lagrangian dynamical geography of the Gulf of Mexico over climatological timescale. They used all the existing datasets, which include additional drifter trajectories from other observation programs between 1994 and 2016. For their purpose, all the different types of drifters were aggregated into one category in order to obtain a sufficient coverage of the whole Gulf of Mexico. The difference in our study is that we separate the drifters by type and by season, and focus on transport originating from the DwH platform. The first step of the method is to discretize the Gulf of Mexico in bins approximately 0.15° × 0.15° (~15 km side). Then, for each of the three drifter datasets (GLAD, LASER drogued drifters, LASER undrogued drifters), a matrix of transitional probabilities of the drifters moving between each bin of the grid is constructed using one-day long trajectory pieces. Once the transitional matrices are calculated, we can map the forward evolution of the probability density of drifters from the location of the DwH platform. The results applied to GLAD and LASER undrogued and drogued drifters are presented in Fig. 8 top right, bottom left, and bottom right panels respectively. To visualize its temporal evolution, the drifter density after 30 days is color coded and contoured in gray line, while the drifter density after one week is only contoured in dotted black. DwH location is marked by a red cross. The top left panel shows for comparison the cumulative days of surface oil detected by SAR-TCNNA analysis during the oil spill in 2010. Note that the oil leaked from a subsurface release for 87 consecutive days reaching the surface in different locations, while the probabilistic transit model simulates an instantaneous release, from one location only, from where advection is averaged over the environmental conditions that occurred during each experiment. With that in mind, the method is based on field data and conditions representative of the seasonality in the Gulf of Mexico, therefore it allows to clearly highlight distinctive transport pathways that occurred as a function of the drifter draft and season.

First, we compare the panels in the top row, where the environmental conditions were similar (summer of 2010 and 2012) but the transport is represented at different depths: the oil slick is at the surface (top left), and the drifters are at 0.5 m depth. The size and shape of the distribution of tracers are quite similar. The maximum density and residence time are found along a southwest-northeast axis passing through DwH. Over the deep ocean (approximately south of DwH), both tracers are entrained in a mesoscale jet related to the Loop Current Eddy system forming the so-called tiger tail that extends towards the south-east. Transport associated with the 2010 and 2012 mesoscale tiger tail features are described in details in Olascoaga and Haller (2012) and Olascoaga et al. (2013). Over the shelf, both tracers spread along the south-west north-east axis, but GLAD drifters spread is reduced in comparison to the oil, and most importantly the drifters remain further offshore than the oil.

Next, we look at the panels in the second row, both corresponding to the winter of 2016, at the surface (bottom left panel undrogued drifters) and near the surface (bottom right panel drogued drifters). The tracer distributions evolve at different rates and follow distinct patterns. After a week, the undrogued drifters (left) have already reached the southern coast of Louisiana, extending 2° further west and 1° further east than the drogued drifters. After a month, two main pathways appear for the

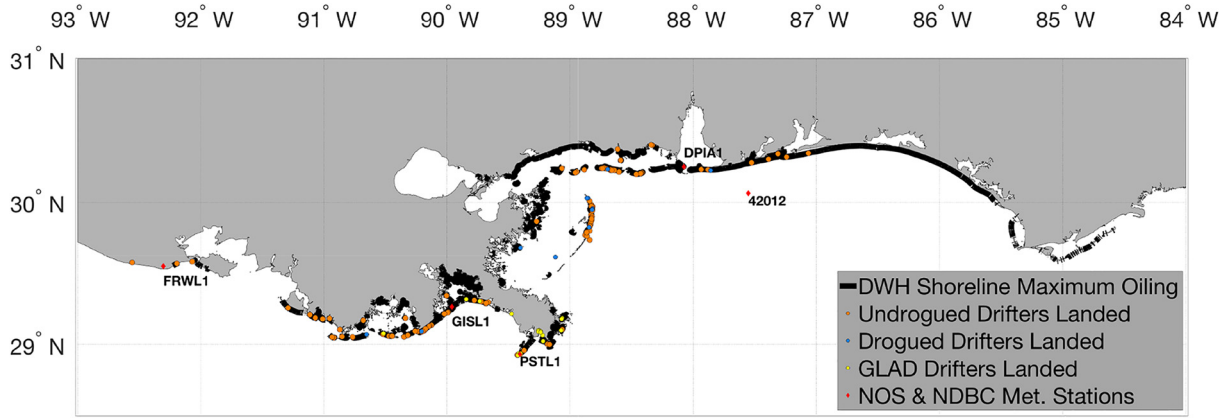

Fig. 9. DwH shoreline oiling is consistent with land fall positions of undrogued drifters. Landing locations of oil (black) from Deepwater Horizon 2010, CODE drifters (yellow, n = 17) from GLAD 2012, drogued (blue, n = 12) and undrogued (orange, n = 108) CARTHE drifters from LASER 2016. Red diamonds mark the locations of NOAA NDBC meteorological stations used in this study for wind speed and wind direction assessment during the landing of the drifters. The black areas mark the location of heavy to light shoreline oiling as assessed by NOAA's Shoreline and Cleanup Assessment Team in September 2010 report (Michel et al., 2013). (For interpretation of the references to color in this figure legend, the reader is referred to the web version of this article.)

Table 2
Number of drifters per region categorized by depth, as they move across the shelf from the deep ocean to shore.

Drifter/experiment	Total	Deep ocean depth: > 300 m	Inner shelf or shelf slope depth: 0 to 300 m	Inner shelf depth: 0 to 50 m	Landed
CODE/GLAD	297	296	166	68	17
CARTHE drogued/LASER	535	535	357	108	21
CARTHE undrogued/LASER	467	405	369	287	115

undrogued drifters: to the west along the shelf as far offshore Galveston Bay, Texas; to the south, as far as 24 N carried by a mesoscale jet, with drifters escaping this jet to the west and circulating around a large anticyclonic eddy centered around (27N; 91W). A few drifters also make it north in the Chandeleur sound region. The drogued drifters propagate mostly along a north-south axis: there is one path to the north over the shelf, towards the Chandeleur Islands and just offshore of the coast of Mississippi and Alabama. The other route is due south and it ends at a bifurcation point where some drifters move east and north, while others go west following the shelf slope. Some drogued drifters were also entrained to the west towards Galveston, but many more undrogued drifters made it to the Louisiana-Texas shelf. Two areas along the shelf slope accumulate drogued drifters (dark shades of orange to black): one slightly west of DwH (28.74N; 88.37W) with a 30-km radius, and one around (24N; 89W). Those are also bifurcation points, where drifters have to pass by before being exported in one direction or another.

Then, we compare panels vertically, that is for similar depth we examine the seasonal transport patterns. Starting on the right side with GLAD (top - summer of 2012) and LASER (bottom - winter of 2016) drogued drifters. In both cases, the near surface drifters are transported far in the deep Gulf along persistent jets, probably associated to the Loop Current Eddy system: pairs of mesoscale counter-rotating eddies can form jets that can efficiently export water masses offshore from the shelf far south in the middle of the Gulf in a few weeks. Over the shelf, the drogued drifters are comparatively slower and the transport is more directed along-shore than across-shore. There is a "parking" area around DwH, with three exit pathways: south into the deep Gulf, north, along the north-eastern coast of Louisiana, and west along the Louisiana-Texas shelf. Similarly, Androulidakis et al. (2018), in their field campaign studying the influence of the Mississippi river-induced fronts on surface transport, found the same three possible exit routes for surface drifters released from the Taylor Energy site, located more onshore than DwH, 17 km East of the South pass of the Mississippi River delta, at a depth of 150 m of water.

Finally, we compare the two panels on the left, the DwH oil slick (summer of 2010) with the LASER undrogued drifters (winter of 2016). Following the summer wind pattern, the oil slick moved generally to the north and to the east. In winter, the undrogued drifters moved more to the west and to the south.

3.4. Landfall of oil and drifters

Fig. 9 shows the locations where DwH oil, GLAD, and LASER drifters, ended stranded along the shorelines of Louisiana, Mississippi, and Florida. A few LASER drifters were also found ashore south of Galveston Bay, Texas, and on the Florida Keys (which can be seen in Fig. 7). The drifters are considered landed when they stopped moving in 5 m of water or less, based on the bathymetry from the Global Self-consistent Hierarchical High-resolution Shorelines database (Wessel and Smith, 1996).

Beached oil that was observed by the SCAT teams appears in black in this map. According to Michel et al. (2013) the Shoreline an Cleanup Assessment Technique teams surveyed over 7000 km of shoreline, 1773 km of which were oiled to some degree (from trace to heavy). Nixon et al. (2016) extended the shoreline assessment database including some oil that landed along the Texas coast along Galveston Bay. Notably, no oil was observed in Atchafalaya Bay (directly East of FRWL1 station in Fig. 9), in the eastern part of the Louisiana Bight (between GISL1 and PSTL1), and on the northern shore of the Mississippi River delta. Quite remarkably, the CARTHE undrogued drifters landed in the same locations where oil was found. Although, none of the undrogued drifters reached the coast to the East of Pensacola, Florida, but oil did: as seen previously in the previous section, the seasonal winter winds pushed the undrogued drifter more to the West of DwH compared to DwH oil spill in the summer of 2010. These observations indicate that the landing locations are not only related to the direction of the seasonal winds with respect to the shoreline orientation, but they also depend on other more permanent features such as the presence of a river mouth, capable of shielding some areas from incoming material (Androulidakis et al., 2018; Roth et al., 2017), and land topography. A fairly small number of the CARTHE drogued drifters and the CODE drifters from GLAD landed as well in more restricted locations, mostly along the Chandeleur barrier islands and at the extremity of the Mississippi River Delta.

Table 2 illustrates the flux of drifters across the shelf from the deep ocean to the coast and summarizes how many drifters landed. Only 17 out of 297 GLAD drifters got stranded (5.7%), 14 of them under 40 m/s winds during the passage of Hurricane Isaac on the 30 August 2012. Similarly, only 21 of the 535 LASER drogued drifters (3.9%) landed. It comes to show that drogued drifters rarely land, with a pattern that is persistent across different seasons. By contrast, 115 of the 467 (24.6%) LASER undrogued drifters found their way to shore. There is a striking difference of fate for surface and near-surface drifters, with a chance of landing 4 to 6 fold higher for surface ones compared to sub-surface ones.

About 60% of the undrogued drifters went from the deep ocean to the inner shelf (this accounts for the fact that ~40 undrogued drifters started their journey on the inner shelf, and ~20 started on the shelf slope), but only 20% of the drogued drifters managed to cross the shelf-slope (from either GLAD or LASER). Further, 40% of the undrogued drifters that were on the inner shelf made it to land, twice as much as the drogued drifters from LASER and GLAD. The contour and slope of the shelf constituted an efficient barrier to cross-slope transport up to the uppermost meter of the ocean sampled by the drogued drifters, both in summer and winter conditions. Mostly constrained by geostrophic currents, drogued drifters hardly moved across the isobaths. However, the motion of the undrogued drifters in the uppermost centimeters of the water column is more subject to surface currents induced by wind and waves. The temporal variability of wind direction and speed, and associated waves, eventually leads to surface transport across the isobaths.

Fig. 10 compares the drifter velocity distribution of drogued and undrogued drifters on the shelf, in less than 50 m depth during the LASER experiment. On the shelf, the mean zonal (positive eastward, Fig. 10 top panel) and meridional (positive northward, Fig. 10 bottom panel) undrogued drifter velocities are −10.8 cm/s and 4.6 cm/s, about twice faster along-shore than across-shore. The mean zonal and meridional drogued drifter velocities are −6.9 cm/s and 2.2 cm/s, about three times faster along-shore than across-shore. Therefore, on the shelf, the undrogued drifters move in average 1.5 and 2 times faster than drogued drifters in the along- and across-shore directions.

The skewness of the zonal velocities, of both drogued and undrogued drifters, to the west represents the westward jet that often

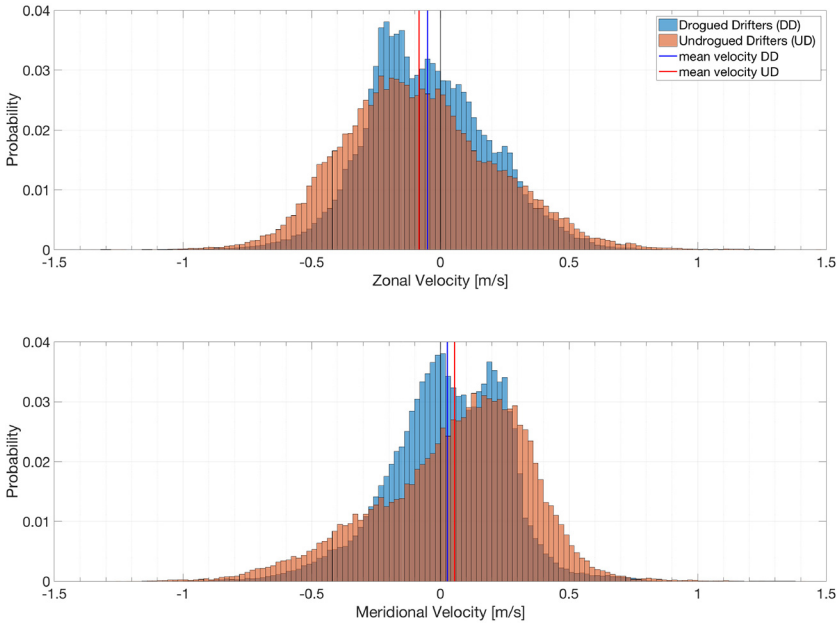

Fig. 10. Probability distributions of zonal (top panels) and meridional (bottom panels) drifter velocities on the shelf (less than 50 m deep) during the LASER experiment. The mean velocities are shown in vertical lines, blue for drogued drifters and red for undrogued drifters. (For interpretation of the references to color in this figure legend, the reader is referred to the web version of this article.)

forms over the Louisiana-Texas shelf (Walker et al., 2005). Both drifter types show a peak at 18 to 20 cm/s in the distribution of the meridional velocities. This northward motion help trap the drifters on the shelf. It could be due to coastal downwelling associated with the dominating easterly winds during the experiment, as seen as well in previous studies of the Mississippi river plume dynamics (Schiller et al., 2011).

4. Discussion

Drifter trajectories and meteorological time-series recorded during the LASER experiment are used to investigate which mechanisms might have led the drifters ashore along the coasts of Louisiana, Mississippi, and Alabama. Fig. 11 focuses on the wind and tidal elevation data recorded at Dauphin Island meteorological station (DPIA1) during the two main drifter stranding events of the LASER dataset that occurred between 09 March 2016 and 02 April 2016. The wind and tidal signals were similar at the other four stations and are not shown here. Between March 09 and March 20, 87 undrogued drifters and 2 drogued drifters came ashore (Fig. 11 bottom panel). The winds were blowing from the east from March 08 to March 13, then winds shifted towards the South until March 18 (Fig. 11 top panel). From March 19 to March 22, a typical winter cold front swept over the Gulf bringing strong northerly winds. No drifter landed between March 20 and March 27. From March 23 to April 02, the dominant pattern of south-easterly winds was re-established. Between March 27 and April 02, 16 undrogued drifters and 10 more drogued drifters became stranded. Previous observational and modeling studies of shelf circulation (Schiller et al., 2011; Walker et al., 2005) have shown that along-shore easterly winds promote downwelling on the inner shelf of the northern Gulf of Mexico. After the passage of cold fronts, north-easterly winds intensify westward surface

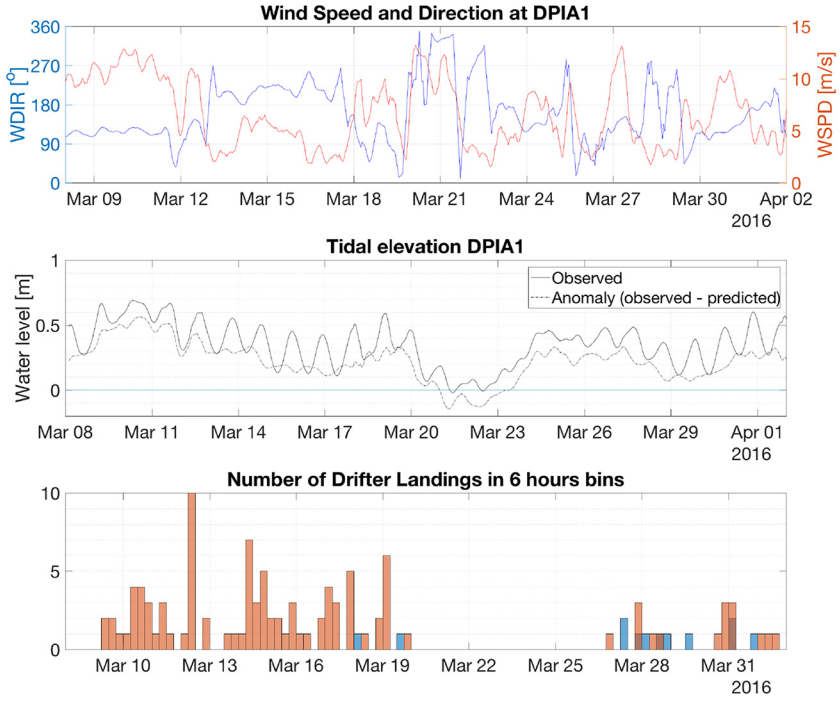

Fig. 11. Top: Wind speed (red line) and wind direction (blue line) at Dauphin Island station DPIA1. Center: Tidal elevation at DPIA1. Bottom: Number of drifter landings in 6 h bins during the main stranding period of LASER (blue for drogued drifters and red for undrogued drifters). (For interpretation of the references to color in this figure legend, the reader is referred to the web version of this article.)

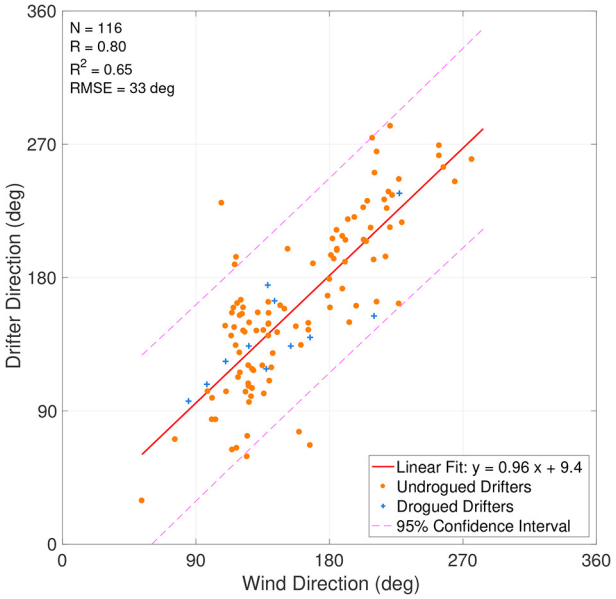

Fig. 12. Scatter plots of direction (coming from) of the wind and the drifters when drifters are reaching land during LASER (March 2016). Comparison statistics are given in the upper left, the best-fit line is shown in red and the 95% confidence interval is shown in dashed magenta lines. (For interpretation of the references to color in this figure legend, the reader is referred to the web version of this article.)

currents. The downwelling was found to drive offshore, low salinity, river plume water near-shore. Similarly, in the observations presented here, a few days of sustained easterly winds tend to bring the drifters to shore. Note, as well, that the easterly winds were associated with a high anomaly of the water level (up to 0.5 m, Fig. 11 middle panel), which indicates that water masses were significantly pushed towards the shore. Soon after, the winds switched direction, from easterly to southerly, and established wind- and wave-induced northward surface currents that enabled drifters to move towards the shore, while maintaining a high tidal elevation. These compounding effects of alongshore easterly winds and onshore sea level rise, followed by southerly wave-induced surface currents, resulted in massive landing of surface drifters. Conversely, the abrupt passage of the northerly cold front wind reversed the direction of the surface currents, and reduced the tidal elevation, which had a double effect: first, drifters were taken away from shore and accelerated their westward export, and second, the recently stranded drifters could not be remobilized by the tide because of the lowered level of the tide line. When winds turned back to easterly, the landings of drifters began again.

Finally, we plot in Fig. 12 the scatter between drifter direction and wind direction in the 15 min preceding the drifters running aground. We compare the direction of each drifter to the wind direction at the closest meteorological station shown in Fig. 9. Winds coming from the South and particularly from the South-East are the most favorable conditions for the landing of drifters. Northerly winds did not result in any landing. Out of 116 landing drifters data points, a robust linear relationship, with a strong positive correlation (R = 0.80), can be traced between the wind direction (WDIR) and the drifter direction (D-DIR) at landing, such that: D-DIR = 0.96 WDIR + 9.4.

There is still a significant spread in drifter direction with respect to the wind direction measured by a root-mean-square-error (RMSE) of 33°. Both drogued and undrogued drifters were found to land under these conditions, which suggests that windage on the drifters is not the only reason that drifters came ashore. The relatively large RMSE could be related to wave-induced transport by Stokes drift and wave-breaking. When waves propagate over shallow water, the local bathymetry causes the waves to steepen (shoaling) and naturally re-orient across the isobaths (diffraction). Sobey et al. (1997) showed that, even in the presence of an along-shore current, the surface velocity induced by the wave field is always directed towards fringing beaches. Furthermore, breaking waves can increase up to ten fold the horizontal transport of surface material, compared to Stokes drift alone (Deike et al., 2017). Therefore, the wave-induced transport is compatible with our observations of drifters landing in the general direction of the wind with a direction RMSE of 33°. The results of our wave-tank experiment support the idea that when Stokes drift is a dominant forcing for the transport of surface drifters, then it plays the same role for the transport of oil slicks. This is in qualitative agreement with the conclusions of numerical studies by Le Hénaff et al. (2012) and Weisberg et al. (2017), which showed that the motion of the DwH oil spill towards the shorelines could not be simulated without including wave-induced drift in these transport models.

5. Conclusions

Much of marine oil spills resides at the surface of the ocean. Wind, waves, and ocean currents can transport and spread oil slicks over large distances until they eventually threaten the coast. Large deployments of GPS-tracked drifters can be an efficient way to simulate oil spills and evaluate theories and models trying to predict the fate of oil spills. This study was carried out to compare the dynamics of oil slicks and different types of drifters, first in a controlled flow in a laboratory and then at large scale in ocean conditions in the Gulf of Mexico.

Steep waves, generated with a paddle in the large OHMSETT tank, allowed to simulate and measure the transport of surface materials induced predominantly by waves. Albeit a small scale simplified version of surface ocean flow, the vertical shear induced by the passage of waves was sufficient to separate, in seconds, the drogued drifter from the oil slick, thin surface bamboo plates, and undrogued drifters. The crude oil and surface drifters were advected at comparable speeds, within 5 to 7%, while the drogue drifter remained still, anchored in a 0.60-m deep layer of water unaffected by the surface Stokes drift. The oil slick and surface drifters patches also stretched at the same rates and in the same principal direction of elongation, within 3°. However, the fresh oil did spread as well across the principal direction. Isotropic spreading is be expected for fresh oil slicks subjected to the balance of gravity, viscosity, and surface tension forces. Such forces do not apply to drifters, which cannot represent this spreading mode of freshly spilled oil.

The second part of this work synthesizes data from one of the largest oil spill in history, and from two large drifter experiments, GLAD and LASER, conducted in the wake of the Deepwater Horizon oil spill. Transport pathways for different seasons were compared based on high resolution (on the order of 10 m and 15 min) field observations compiling 1299 drifter trajectories that lasted for months and thousands of kilometers across the Gulf of Mexico. The same drogued and undrogued drifters used in the laboratory experiment sampled at two different depths relevant to the oil transport -the upper 0.05 m and the upper 0.50 m. Their trajectories revealed a great contrast between transport patterns and timescales as a function of depth. Landing patterns were also analyzed for the first time.

The density of drifter data near the Deepwater Horizon platform is high enough to build probabilistic transport models originating from the source of the spill. These data-based models clearly show long residence time in the Deepwater Horizon area where the shelf slope is narrow, and three exit paths: one towards the south and deeper Gulf via entrainment in persistent jets, presumably formed in between mesoscale eddies of the Loop Current Eddy system; the two other routes pass over the inner shelf, either to the east or to the west of the Mississippi delta. Only 20% of the drogued drifters are able to cross the shelf slope, against 60% of the undrogued ones. The variability of surface winds, and associated waves, by inducing surface currents, as well as directly acting on the surface material (oil or undrogued

drifters), may explain the surface transport observed across the isobaths.

In both summer and winter, the surface transport over the shelf was controlled by the coastal winds. Onshore winds and associated wind-waves Stokes drift, as well as sustained easterly along-shore winds accompanied by coastal sea level rise, were responsible for bringing drifters all the way to the shore. Conversely, during periods of offshore winds and westerly along-shore winds, the circulation over the shelf reversed and no drifter landing occurred. Over the inner shelf, surface undrogued drifters were transported towards the shore twice as fast as near-surface drifters. This corroborates, and extends, previous observations of intense near-surface vertical shear made in the Louisiana Bight (Laxague et al., 2018).

Undrogued drifters also had 5 to 6 times more chances of landing than the drogued drifters. The drogued near-surface drifters rarely landed, but most of them did during a hurricane or when the wind was directed onshore and the wind speed was higher than 8 m/s. The undrogued drifters remarkably landed in the same locations where Deepwater Horizon oil did. Wave-tank experiments demonstrated that oil slicks were transported by waves-induced Stokes drift like surface undrogued drifters and bamboo plates. Therefore, near-shore wave-induced drift (via Stokes drift and wave-breaking) is potentially a major mechanism that leads to the stranding of drifters and oil.

No oil nor drifters landed along the closest western coastlines adjacent to the Mississippi River delta and the Atchafalaya River, in agreement with other observations of river plume fronts temporarily protecting a river mouth from the landing of flotsam (Androulidakis et al., 2018; Roth et al., 2017). However, sustained alongshore winds could still cause these fronts, and the surface material accumulated along them, to move either onshore under easterly winds (more typical of winter) or offshore under westerly winds (more typical of summer).

The experiments conducted in the wave-tank help explain the cross-shore transport of surface material observed in the field. They demonstrate that the near-surface current shear, induced by winds and high-frequency wind-waves, can lead to efficient transport across the shelf, and affects where and when landfall may occur.

It was not possible to estimate the direct effect of wind, commonly called windage, on oil and undrogued drifters. That would require careful measurements of wind and surface currents along oil and drifter trajectories. However, all the observations presented here support that the large scale transport mechanisms for both oil slicks and undrogued drifters may be the same. One of the implication of this work could be to recommend the use of both drogued and undrogued drifters as oil surrogates for environmental impact assessment and contingency planning experiments. Various numerical models are used to study the transport of other surface material of interest such as floating algae, fish eggs, or plastic debris. The evaluation of such models could benefit from comparison with large drift datasets like the ones used here that include collocated, drogued and undrogued, drifter trajectories.

CRediT authorship contribution statement

Guillaume Novelli: Conceptualization, Investigation, Software, Formal analysis, Data curation, Visualization, Writing - original draft, Writing - review & editing. **Cédric M. Guigand:** Methodology, Investigation, Data curation, Writing - review & editing. **Michel C. Boufadel:** Investigation, Supervision, Writing - review & editing. **Tamay M. Özgökmen:** Conceptualization, Investigation, Writing - original draft, Writing - review & editing, Funding acquisition, Supervision.

Declaration of competing interest

The authors declare that they have no known competing financial interests or personal relationships that could have appeared to influence the work reported in this paper.

Acknowledgments

This research was made possible by a grant from the Gulf of Mexico Research Initiative. Data are publicly available through the Gulf of Mexico Research Initiative Information and Data Cooperative (GRIIDC) at https://data.gulfresearchinitiative.org under doi:10.7266/N7Z89B0D (OHMSETT experiment); doi:10.7266/N7W0940J (LASER drifter data); doi: 10.7266/N7VD6WC8 (GLAD drifter data).

Deepwater Horizon oiling data are publicly available from the Environmental Response Management Application (ERMA) Gulf of Mexico at https://erma.noaa.gov/gulfofmexico/erma.html.

Standard meteorological data time-series at stations FRWL1, PSTL1, GISL1, DPIA1, and 42012, are collected by NOAA's National Data Buoy Center and publicly accessible at: https://www.ndbc.noaa.gov.

We are thankful for the OHMSETT personnel for their expert help in setting up the wave-tank experiment. The drifter deployments would not have been possible without the dedication of tens of technicians and scientists of the CARTHE team over years.

References

Androulidakis, Y., Kourafalou, V., Garcia, O., Hu, C., Haus, B.K., Novelli, G., Guigand, C., Kang, H., Hole, L., 2018. Influence of river induced fronts on hydrocarbon transport: a multi-platform observational study. J. Geophys. Res. Oceans 1–70. https://doi.org/10.1002/2017JC013514. https://agupubs.onlinelibrary.wiley.com/doi/epdf/10.1029/2017JC013514.

Beron-Vera, F.J., LaCasce, J.H., 2016. Statistics of simulated and observed pair separations in the Gulf of Mexico. J. Phys. Oceanogr. 46, 2183–2199. https://doi.org/10.1175/JPO-D-15-0127.1. http://arxiv.org/abs/1505.03475{\%}0A arXiv:1505.03475.

Berta, M., Griffa, A., Magaldi, M.G., Özgökmen, T.M., Poje, A.C., Haza, A.C., Josefina Olascoaga, M., 2015. Improved surface velocity and trajectory estimates in the Gulf of Mexico from blended satellite altimetry and drifter data. J. Atmos. Ocean. Technol. 32, 1880–1901. https://doi.org/10.1175/JTECH-D-14-00226.1.

Boufadel, M.C., Gao, F., Zhao, L., Özgökmen, T., Miller, R., King, T., Robinson, B., Lee, K., Leifer, I., 2018. Was the Deepwater Horizon well discharge churn flow? Implications on the estimation of the oil discharge and droplet size distribution. Geophys. Res. Lett. 45, 2396–2403. https://doi.org/10.1002/2017GL076606.

Carlson, D.F., Ozgokmen, T.M., Novelli, G., Guigand, C.M., Chang, H., Fox-kemper, B., Mensa, J., Mehta, S., Fredj, E., Huntley, H.S., Kirwan, A.J., Berta, M., Rebozo, M., Curcic, M., Ryan, E.H., Lund, B., Molemaker, M.J., D'Asaro, E.A., Haus, B.K., Hunt, C., Chen, S.S., Bracken, L., Dalziel, S., Hortsmann, J., 2018. Near-surface dispersion observations from the ship-tethered aerostat remote sensing system. Front. Mar. Sci. 1–35.

Clarke, A.J., Van Gorder, S., 2018. The relationship of near-surface flow, Stokes drift and the wind stress. J. Geophys. Res. Oceans 123, 4680–4692. https://doi.org/10.1029/2018JC014102.

Curcic, M., Chen, S.S., Özgökmen, T.M., 2016. Hurricane-induced ocean waves and stokes drift and their impacts on surface transport and dispersion in the Gulf of Mexico. n/a–n/a. Geophys. Res. Lett. 43. https://doi.org/10.1002/2015GL067619.

Daling, P.S., Moldestad, M.Ø., Johansen, Ø., Lewis, A., Rødal, J., 2003. Norwegian testing of emulsion properties at sea-the importance of oil type and release conditions. Spill Sci. Technol. Bull. 8, 123–136. https://doi.org/10.1016/S1353-2561(03)00016-1.

D'Asaro, E.A., Shcherbina, A.Y., Klymak, J.M., Molemaker, J., Novelli, G., Guigand, C.M., Haza, A.C., Haus, B.K., Ryan, E.H., Jacobs, G.A., Huntley, H.S., Laxague, N.J.M., Chen, S., Judt, F., McWilliams, J.C., Barkan, R., Kirwan, A.D., Poje, A.C., Özgökmen, T.M., 2018. Ocean convergence and the dispersion of flotsam. Proc. Natl. Acad. Sci. 201718453. https://doi.org/10.1073/pnas.1718453115. http://www.pnas.org/lookup/doi/10.1073/pnas.1718453115.

Davis, R.E., 1985. Drifter observations of coastal surface currents during CODE: the method and descriptive view. J. Geophys. Res. 90, 4741–4755.

Deike, L., Pizzo, N., Melville, W.K., 2017. Lagrangian transport by breaking surface waves. J. Fluid Mech. 829, 364–391. https://doi.org/10.1017/jfm.2017.548.

Drennan, W., Graber, H., Donelan, M., Terray, E., 1998. Directional wave measurements from the ASIS (Air-Sea Interaction Spar) buoy. Nice In: IEEE Oceanic Engineering Society OCEANS'98, pp. 414–418. https://doi.org/10.1109/oceans.1998.725779. http://ieeexplore.ieee.org/stamp/stamp.jsp?tp=&arnumber=725779&isnumber=15668.

Faksness, L.G., Brandvik, P.J., Daling, P.S., Singsaas, I., Sørstrøm, S.E., 2016. The value of offshore field experiments in oil spill technology development for Norwegian waters. Mar. Pollut. Bull. 111, 402–410. https://doi.org/10.1016/j.marpolbul.2016.07.035.

Fay, J.A., 1971. Physical processes in the spread of oil on a water surface. In: Proceedings of the Joint Conference on Prevention and Control of Oil Spills, Washington, D.C., June, pp. 463–467.

Fingas, M.F., 2011. Buoys and devices for oil spill tracking Merv Fingas Spill Science, Edmonton, Alberta Canada. Proceedings of the Thirty-fourth AMOP Technical Seminar on Environmental Contamination and Response 5.

Garcia-Pineda, O., MacDonald, I.R., Li, X., Jackson, C.R., Pichel, W.G., 2013. Oil spill mapping and measurement in the Gulf of Mexico with Textural Classifier Neural

Network Algorithm (TCNNA). IEEE J. Sel. Top. Appl. Earth Obs. Remote Sens. 6, 2517–2525. https://doi.org/10.1109/JSTARS.2013.2244061.
Garcia-Pineda, O., Zimmer, B., Howard, M., Pichel, W., Li, X., MacDonald, I.R., 2009. Using SAR images to delineate ocean oil slicks with a texture-classifying neural network algorithm (TCNNA). Can. J. Remote. Sens. 35, 411–421. https://doi.org/10.5589/m09-035.
Goodman, R.H., Simecek-Beatty, D., Hodgins, D., 1995. Tracking buoys for oil spills. In: Proc. 1995 Int. Oil Spill Conf. pp. 523–534.
Haza, A.C., D'Asaro, E., Chang, H., Chen, S., Curcic, M., Guigand, C., Huntley, H.S., Jacobs, G., Novelli, G., Özgökmen, T.M., Poje, A.C., Ryan, E., Shcherbina, A., 2018. Drogue-loss detection for surface drifters during the Lagrangian Submesoscale Experiment (LASER). JTECH-D-17-0143.1. J. Atmos. Ocean. Technol. https://doi.org/10.1175/JTECH-D-17-0143.1. http://journals.ametsoc.org/doi/10.1175/JTECH-D-17-0143.1.
Hoult, D.P., 1972. Oil spreading on the sea. Annu. Rev. Fluid Mech. 341.
Hu, C., Weisberg, R.H., Liu, Y., Zheng, L., Daly, K.L., English, D.C., Zhao, J., Vargo, G.A., 2011. Did the northeastern Gulf of Mexico become greener after the Deepwater Horizon oil spill? Geophys. Res. Lett. 38 (9), 1–5. https://doi.org/10.1029/2011GL047184.
Jones, C.E., Dagestad, K.-F., Breivik, Ø., Holt, B., Röhrs, J., Christensen, K.H., Espeseth, M., Brekke, C., Skrunes, S., 2016. Measurement and modeling of oil slick transport. J. Geophys. Res. Oceans 121, 3372–3380. https://doi.org/10.1002/2015JC011421.Received.
Judt, F., Chen, S.S., Curcic, M., 2016. Journal of Geophysical Research: Oceans. J. Geophys. Res. Oceans 121, 4416–4433. https://doi.org/10.1002/2015JC011555.
LaCasce, J.H., 2008. Statistics from Lagrangian observations. Prog. Oceanogr. 77, 1–29. https://doi.org/10.1016/j.pocean.2008.02.002.
Laxague, N., Özgökmen, T., Haus, B., Novelli, G., Shcherbina, A., Sutherland, P., Guigand, C., Lund, B., Mehta, S., Alday, M., Molemaker, J., 2018. Observations of near-surface current shear help describe oceanic oil and plastic transport. Geophys. Res. Lett. 45. https://doi.org/10.1002/2017GL075891.
Laxague, N.J., Haus, B.K., Ortiz-Suslow, D.G., Smith, C.J., Novelli, G., Dai, H., Özgökmen, T., Graber, H.C., 2017. Passive optical sensing of the near-surface wind-driven current profile. J. Atmos. Ocean. Technol. 34, 1097–1111. https://doi.org/10.1175/JTECH-D-16-0090.1.
Le Hénaff, M., Kourafalou, V.H., Paris, C.B., Helgers, J., Aman, Z.M., Hogan, P.J., Srinivasan, A., 2012, jul, jul. Surface evolution of the Deepwater Horizon oil spill patch: combined effects of circulation and wind-induced drift. Environ. Sci. Technol. 46, 7267–7273. https://doi.org/10.1021/es301570w. http://www.ncbi.nlm.nih.gov/pubmed/22676453.
Mariano, A., Ryan, E., Huntley, H., Laurindo, L., Coelho, E., Griffa, A., Ozgökmen, T.M., Berta, M., Bogucki, D., Chen, S.S., Curcic, M., Drouin, K., Gough, M., Haus, B., Haza, A.C., Hogan, P., Iskandarani, M., Jacobs, G., Kirwan, A.J., Laxague, N.J., Lipphardt, B., Magaldi, M.G., Novelli, G., Reniers, A.J., Restrepo, J.M., Smith, C.J., Valle-Levinson, A., Wei, M., 2016. Statistical properties of the surface velocity field in the northern Gulf of Mexico sampled by GLAD drifters. J. Geophys. Res. Oceans 121, 5193–5216. https://doi.org/10.1002/2015JC011486.Received.
Mariano, A.J., Kourafalou, V.H., Srinivasan, A., Kang, H., Halliwell, G.R., Ryan, E.H., Roffer, M., 2011. On the modeling of the 2010 Gulf of Mexico oil spill. Dyn. Atmos. Oceans 52, 322–340. https://doi.org/10.1016/j.dynatmoce.2011.06.001.
Maximenko, N., Hafner, J., Niiler, P., 2012. Pathways of marine debris derived from trajectories of Lagrangian drifters. Mar. Pollut. Bull. 65, 51–62. https://doi.org/10.1016/j.marpolbul.2011.04.016.
Meijering, E., Dzyubachyk, O., Smal, I., 2012. Methods for cell and particle tracking. Methods Enzymol. 504, 183–200. https://doi.org/10.1016/B978-0-12-391857-4.00009-4. http://www.ncbi.nlm.nih.gov/pubmed/22264535 arXiv:arXiv:1011.1669v3.
Michel, J., Owens, E.H., Zengel, S., Graham, A., Nixon, Z., Allard, T., Holton, W., Reimer, P.D., Lamarche, A., White, M., Rutherford, N., Childs, C., Mauseth, G., Challenger, G., Taylor, E., 2013. Extent and degree of shoreline oiling: Deepwater Horizon oil spill, Gulf of Mexico, USA. PLoS ONE 8, 1–9. https://doi.org/10.1371/journal.pone.0065087.
Miron, P., Beron-Vera, F.J., Olascoaga, M.J., Sheinbaum, J., Pérez-Brunius, P., Froyland, G., 2017. Lagrangian dynamical geography of the Gulf of Mexico. Sci. Rep. 7, 1–12. https://doi.org/10.1038/s41598-017-07177-w. arXiv:1703.10684.
Nixon, Z., Zengel, S., Baker, M., Steinhoff, M., Fricano, G., Rouhani, S., Michel, J., 2016. Shoreline oiling from the Deepwater Horizon oil spill. Mar. Pollut. Bull. 107, 170–178. https://doi.org/10.1016/j.marpolbul.2016.04.003.
Novelli, G., Guigand, C.M., Cousin, C., Ryan, E.H., Laxague, N.J.M., Dai, H., Haus, B.K., Özgökmen, T.M., 2017. A biodegradable surface drifter for ocean sampling on a massive scale. J. Atmos. Ocean. Technol. 34, 2509–2532. https://doi.org/10.1175/JTECH-D-17-0055.1.
Novelli, G., Guigand, C.M., Özgökmen, T.M., 2018. Technological advances in drifters for oil transport studies. Mar. Technol. Soc. J. 52, 53–61.
Olascoaga, M.J., Beron-Vera, F.J., Haller, G., Tri nanes, J., Iskandarani, M., Coelho, E.F., Haus, B.K., Huntley, H.S., Jacobs, G., Kirwan, A.D., Lipphardt, B.L., Özgökmen, T.M., A.J., H.M.Reniers, Valle-Levinson, A., 2013. Drifter motion in the Gulf of Mexico constrained by altimetric Lagrangian coherent structures. Geophys. Res. Lett. 40, 6171–6175. https://doi.org/10.1002/2013GL058624.
Olascoaga, M.J., Haller, G., 2012. Forecasting sudden changes in environmental pollution patterns. Proc. Natl. Acad. Sci. 109, 4738–4743. https://doi.org/10.1073/pnas.1118574109.
Piterbarg, L.I., Ozgokmen, T.M., Griffa, A., Mariano, A.J., 2007. Predictability of the Lagrangian motion in the upper ocean. In: Griffa, A., Kirwan, A.J., Mariano, A., Ozgokmen, T.M., Rossby, T. (Eds.), Lagrangian Analysis and Prediction of Coastal and Ocean Dynamics. Cambridge University Press, pp. 136–172. https://doi.org/10.1017/CBO9780511535901.007. http://adsabs.harvard.edu/abs/2001AGUFMNG42A0407P.
Poje, A.C., Özgökmen, T.M., Lipphardt, B.L., Haus, B.K., Ryan, E.H., Haza, A.C., Jacobs, G.A., Reniers, A.J.H.M., Olascoaga, M.J., Novelli, G., Griffa, A., Beron-Vera, F.J., Chen, S.S., Coelho, E., Hogan, P.J., Kirwan, A.D., Huntley, H.S., Mariano, A.J., 2014. Submesoscale dispersion in the vicinity of the Deepwater Horizon spill. Proc. Natl. Acad. Sci. U. S. A. 111 (35), 12693–12698. https://doi.org/10.1073/pnas.1402452111. arXiv:arXiv:1407.3308v2.
Poulain, P.M., Gerin, R., 2019. Assessment of the water-following capabilities of CODE drifters based on direct relative flow measurements. J. Atmos. Ocean. Technol. 36, 621–633. https://doi.org/10.1175/JTECH-D-18-0097.1.
Reed, M., Johansen, O., Brandvik, P.J., Daling, P., Lewis, A., Fiocco, R., Mackay, D., Prentki, R., 1999. Oil spill modeling towards the close of 20th century: overview of the state of the art. Spill Sci. Technol. Bull. 5, 3–16.
Reed, M., Turner, C., Odulo, A., 1994. The role of wind and emulsification in modelling oil spill and surface drifter trajectories. Spill Sci. Technol. Bull. 1, 143–157. https://doi.org/10.1016/1353-2561(94)90022-1.
Röhrs, J., Christensen, K.H., Hole, L.R., Broström, G., Drivdal, M., Sundby, S., 2012. Observation-based evaluation of surface wave effects on currents and trajectory forecasts. Ocean Dyn. 62, 1519–1533. https://doi.org/10.1007/s10236-012-0576-y.
Roth, M.K., MacMahan, J., Reniers, A., Özgökmen, T.M., Woodall, K., Haus, B., 2017. Observations of inner shelf cross-shore surface material transport adjacent to a coastal inlet in the northern Gulf of Mexico. Cont. Shelf Res. 137, 142–153. https://doi.org/10.1016/j.csr.2016.12.017.
Schiller, R.V., Kourafalou, V.H., Hogan, P., Walker, N.D., 2011. The dynamics of the Mississippi River plume: impact of topography, wind and offshore forcing on the fate of plume waters. J. Geophys. Res. OCEANS. 116, 1–22. https://doi.org/10.1029/2010JC006883.
Schneider, C.A., Rasband, W.S., Eliceiri, K.W., 2012. NIH image to ImageJ: 25 years of image analysis. Nat. Methods 9, 671–675. https://doi.org/10.1038/nmeth.2089. arXiv:arXiv:1011.1669v3.
Sobey, R.J., Barker, C.H., Spring, F., 1997. Wave-driven transport of surface oil. J. Coast. Res. 13, 490–496.
Soloviev, A.V., Haus, B.K., McGauley, M.G., Dean, C.W., Ortiz-Suslow, D.G., Laxague, N.J.M., Özgökmen, T.M., 2016. Surface dynamics of crude and weathered oil in the presence of dispersants: laboratory experiment and numerical simulation. J. Geophys. Res. Oceans 121, 3502–3516. https://doi.org/10.1002/2015JC011533.Received.
Spaulding, M.L., 2017. State of the art review and future directions in oil spill modeling. Mar. Pollut. Bull. 115, 7–19. https://doi.org/10.1016/j.marpolbul.2017.01.001.
Tamura, H., Miyazawa, Y., Oey, L.Y., 2012. The stokes drift and wave induced-mass flux in the North Pacific. J. Geophys. Res. Oceans 117, 1–14. https://doi.org/10.1029/2012JC008113.
Walker, N.D., Jr, W.J.W., Jr, L.J.R., Babin, A., Beach, W.P., Walker, N.D., Jr, W.J.W., Jr, L.J.R., Babin, A., 2005. Effects of river discharge, wind stress, and slope eddies on circulation and the satellite-observed structure of the Mississippi River plume. J. Coast. Res. 21, 1228–1244. https://doi.org/10.2112/04-0347.1.
Wang, Z., Hollebone, B.P., Fingas, M., Fieldhouse, B., Sigouin, L., Landriault, M., Smith, P., Noonan, J., Thouin, G., Weaver, J.W., 2003. Characteristics of spilled oils, fuels, and petroleum products: 1. Composition and properties of selected oils. In: Technical Report July. US EPA, https://doi.org/10.23919/MIPRO.2018.8400058. http://nepis.epa.gov/Adobe/PDF./P1000AE6.pdf{\%}5Cnpapers2://publication/uuid/504BA836-2847-4C34-9BF4-4DA351C932B6{\%}5Cnpapers2://publication/uuid/C0AC5D53-502E-44D7-9EA1-4D8B00FD9C0C.
Weisberg, R.H., Lianyuan, Z., Liu, Y., 2017. On the movement of Deepwater Horizon oil to Northern Gulf beaches. Ocean Model. 111, 81–97. https://doi.org/10.1016/j.ocemod.2017.02.002. arXiv:arXiv:1011.1669v3.
Wessel, P., Smith, W.H.F., 1996. A global, self-consistent, hierarchical, high-resolution shoreline database. J. Geophys. Res. Solid Earth 101, 8741–8743. https://doi.org/10.1029/96JB00104. http://doi.wiley.com/10.1029/96JB00104.
Yaremchuk, M., Coelho, E.F., 2015. Filtering drifter trajectories sampled at submesoscale resolution. IEEE J. Ocean. Eng. 40, 497–505. https://doi.org/10.1109/JOE.2014.2353472.
Zhao, L., Shaffer, F., Robinson, B., King, T., D'Ambrose, C., Pan, Z., Gao, F., Miller, R.S., Conmy, R.N., Boufadel, M.C., 2016. Underwater oil jet: hydrodynamics and droplet size distribution. Chem. Eng. J. 299, 292–303. https://doi.org/10.1016/j.cej.2016.04.061.